Figure S1

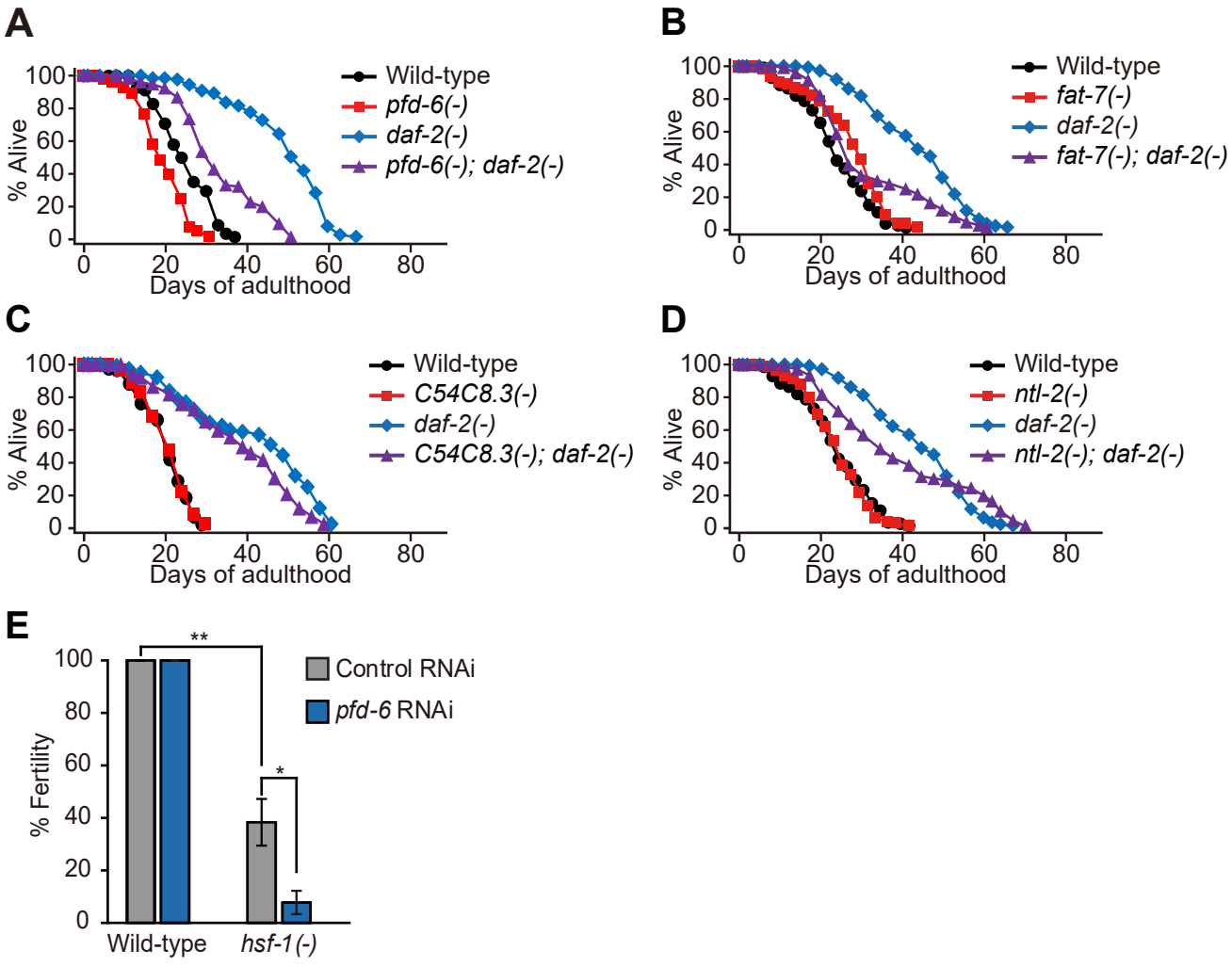
A
% Alive
Days of adulthood
Wild-type
pfd-6(-)
daf-2(-)
pfd-6(-); daf-2(-)
B
% Alive
Days of adulthood
Wild-type
fat-7(-)
daf-2(-)
fat-7(-); daf-2(-)
C
% Alive
Days of adulthood
Wild-type
C54C8.3(-)
daf-2(-)
C54C8.3(-); daf-2(-)
D
% Alive
Days of adulthood
Wild-type
ntl-2(-)
daf-2(-)
ntl-2(-); daf-2(-)
E
% Fertility
Control RNAi
pfd-6 RNAi
Wild-type
hsf-1(-)

Figure S1. The effects of mutations in *pfd-6, fat-7, C54C8.3* or *ntl-2* on lifespan and those of *pfd-6* RNAi on fertility. (**A** and **B**) *pfd-6(gk493446)* (*pfd-6(-)*) (**A**) or *fat-7(wa36)* (*fat-7(-)*) (**B**) mutations partially suppressed the long lifespan of *daf-2(e1370)* (*daf-2(-)*) mutant animals. (**C** and **D**) *C54C8.3(gk896531)* (*C54C8.3(-)*) (**C**) or *ntl-2(gk390728)* (*ntl-2(-)*) (**D**) mutations had small or no effects on the lifespan of wild-type or *daf-2(-)* animals. See **Supplemental Table S2** for statistical analysis and additional repeats. (**E**) Fertility of wild-type and *hsf-1(sy441)* (*hsf-1(-)*) mutant worms treated with control RNAi or *pfd-6* RNAi on solid plates (three biological repeats). Error bars represent SEM (two-tailed Student's *t*-test, $*p < 0.05$, $**p < 0.01$).

Figure S2

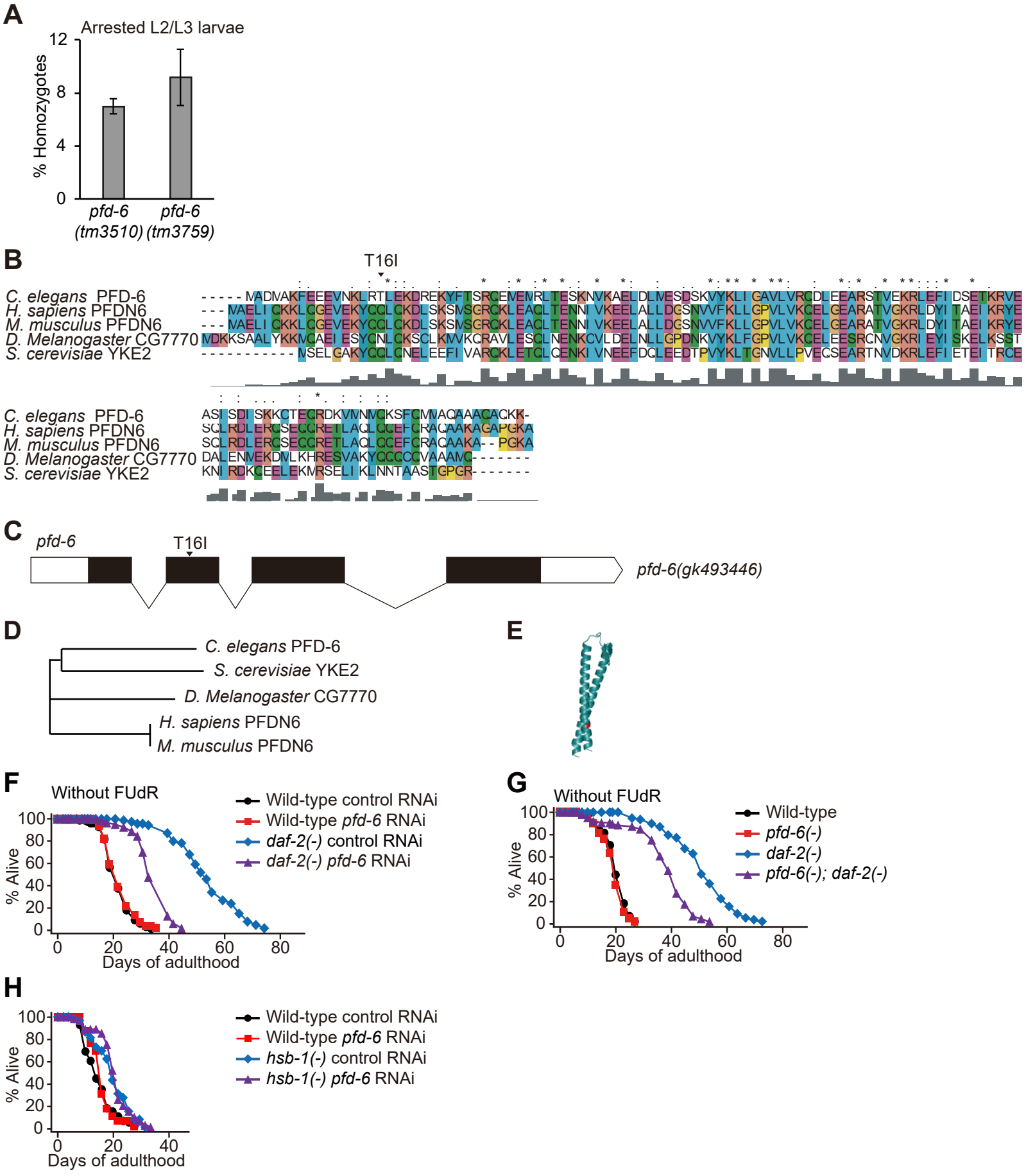
A
Arrested L2/L3 larvae
% Homozygotes
12
8
4
0
pfd-6 (tm3510)
pfd-6 (tm3759)
B
T16I
C. elegans PFD-6
H. sapiens PFDN6
M. musculus PFDN6
D. Melanogaster CG7770
S. cerevisiae YKE2
C
pfd-6
T16I
pfd-6(gk493446)
D
C. elegans PFD-6
S. cerevisiae YKE2
D. Melanogaster CG7770
H. sapiens PFDN6
M. musculus PFDN6
E
F
Without FUdR
% Alive
Days of adulthood
Wild-type control RNAi
Wild-type pfd-6 RNAi
daf-2(-) control RNAi
daf-2(-) pfd-6 RNAi
G
Without FUdR
% Alive
Days of adulthood
Wild-type
pfd-6(-)
daf-2(-)
pfd-6(-); daf-2(-)
H
% Alive
Days of adulthood
Wild-type control RNAi
Wild-type pfd-6 RNAi
hsb-1(-) control RNAi
hsb-1(-) pfd-6 RNAi

Figure S2. Evolutionarily conserved PFD-6 is required for the long lifespan of *daf-2* mutants. (**A**) Percent homozygous *pfd-6* deletion mutants that hatched were measured, by using two strong loss of function alleles of *pfd-6* that are balanced: *pfd-6(tm3759)/hT2[bli-4(e937) let-?(q782) qIs48[Pmyo-2::gfp; Ppes-10::gfp; Pges-1::gfp]]* and *pfd-6(tm3510)/hT2*. All the homozygous mutant worms that hatched arrested as L2 or L3 larvae. Error bars represent SEM using three biological repeats. (**B**) PFD-6 is conserved among various species. Amino acid sequence alignment of *C. elegans* PFD-6, *H. sapiens* PFDN6 (41%), *M. musculus* PFDN6 (41%), *D. melanogaster* CG7770 (36%) and *S. cerevisiae* YKE2 (36%) was generated using Clustal W2 and colored in box shades with asterisks (completely identical residues) or dots (similar or identical residues). (**C**) Shown is a schematic diagram of exon and intron regions of *pfd-6*. *pfd-6(gk493446)* mutation causes an amino acid substitution, T16 to I. (**D**) Phylogenic tree of PFD-6 homologs in *C. elegans*, *D. melanogaster*, *S. cerevisiae*, *M. musculus* and *H. sapiens*. (**E**) Predicted structure of PFD-6 presents a coiled-coil structure that is involved in substrate-binding. (**F** and **G**) *pfd-6* RNAi (**F**) or *pfd-6* mutations (**G**) partially decreased the longevity of *daf-2* mutants in the absence of FUdR. (**H**) *pfd-6* RNAi did not affect the longevity of *hsb-1(cg116)* (*hsb-1(-)*) mutants. See **Supplemental Table S3** for statistical analysis and additional repeats.

Figure S3

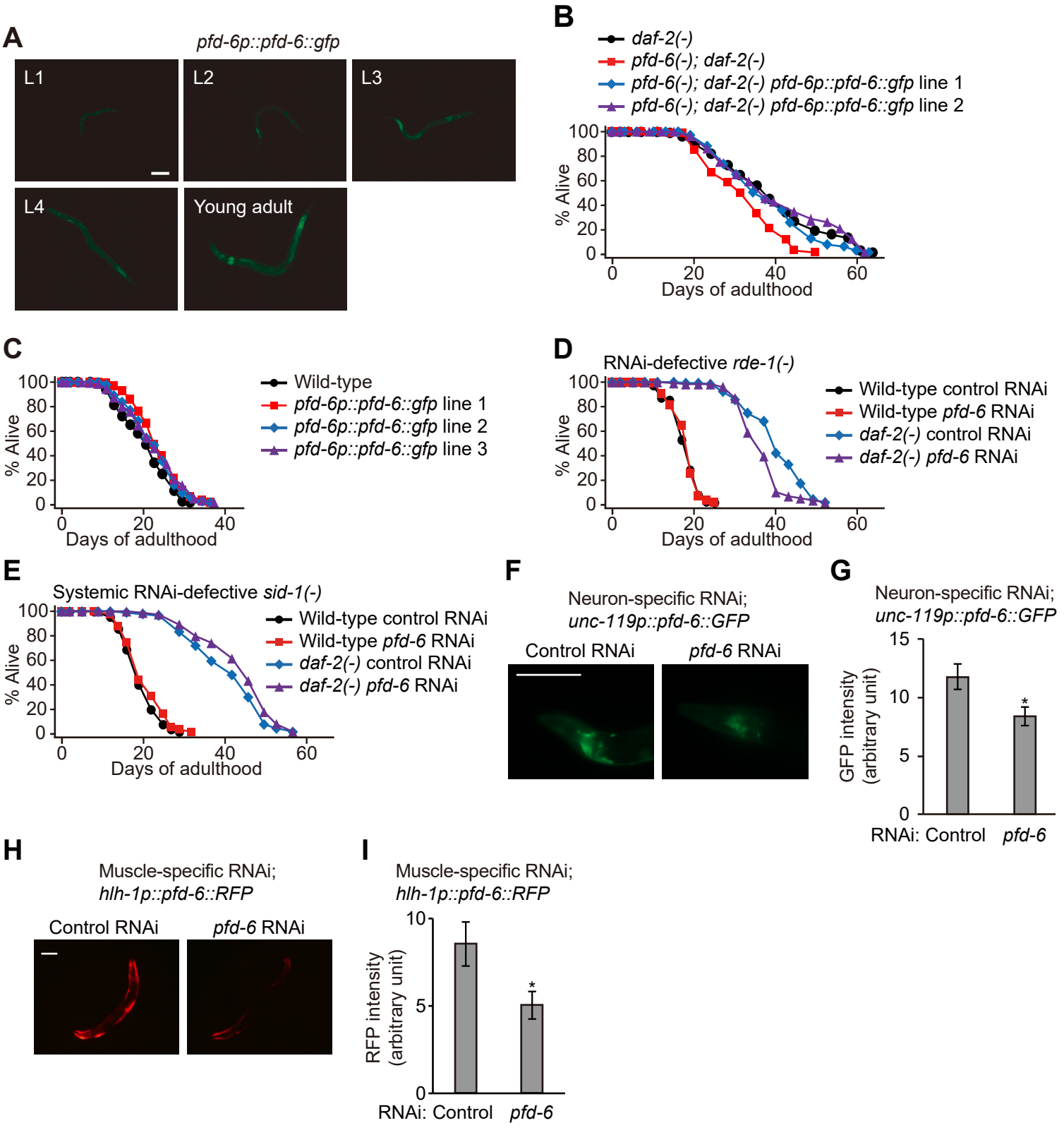
A
pfd-6p::pfd-6::gfp
L1
L2
L3
L4
Young adult
B
daf-2(-)
pfd-6(-); daf-2(-)
pfd-6(-); daf-2(-) pfd-6p::pfd-6::gfp line 1
pfd-6(-); daf-2(-) pfd-6p::pfd-6::gfp line 2
% Alive
Days of adulthood
C
Wild-type
pfd-6p::pfd-6::gfp line 1
pfd-6p::pfd-6::gfp line 2
pfd-6p::pfd-6::gfp line 3
% Alive
Days of adulthood
D
RNAi-defective rde-1(-)
Wild-type control RNAi
Wild-type pfd-6 RNAi
daf-2(-) control RNAi
daf-2(-) pfd-6 RNAi
% Alive
Days of adulthood
E
Systemic RNAi-defective sid-1(-)
Wild-type control RNAi
Wild-type pfd-6 RNAi
daf-2(-) control RNAi
daf-2(-) pfd-6 RNAi
% Alive
Days of adulthood
F
Neuron-specific RNAi;
unc-119p::pfd-6::GFP
Control RNAi
pfd-6 RNAi
G
Neuron-specific RNAi;
unc-119p::pfd-6::GFP
GFP intensity (arbitrary unit)
RNAi: Control
pfd-6
H
Muscle-specific RNAi;
hlh-1p::pfd-6::RFP
Control RNAi
pfd-6 RNAi
I
Muscle-specific RNAi;
hlh-1p::pfd-6::RFP
RFP intensity (arbitrary unit)
RNAi: Control
pfd-6

Figure S3. The expression patterns of *pfd-6* during development and the effect of *pfd-6* transgenes and RNAi on lifespan. (**A**) *pfd-6* was expressed in multiple tissues throughout development (scale bar: 100 μm). (**B**) Two different lines of *pfd-6p::pfd-6::gfp* transgenes restored long lifespan in *pfd-6(gk493446); daf-2(e1370)* (*pfd-6(-); daf-2(-)*) double mutants. (**C**) Three different lines of *pfd-6p::pfd-6::gfp* transgenes marginally affected the lifespan of wild-type. (**D**) *pfd-6* RNAi did not affect the lifespan of RNAi-defective *rde-1(ne219)* (*rde-1(-)*) mutants, but marginally decreased the lifespan of *rde-1(ne219); daf-2(e1370)* (*rde-1(-); daf-2(-)*) mutants (3 out of 4 trials) (**E**) The lifespan of systemic RNAi-defective *sid-1(pk3321)* (*sid-1(-)*) or *daf-2(e1370); sid-1(pk3321)* (*daf-2(-); sid-1(-)*) mutants was not changed by *pfd-6* RNAi. See **Supplemental Table S4** for statistical analysis and additional repeats. (**F**) Fluorescence images of *unc-119p::pfd-6::GFP* worms in neuron-specific RNAi backgrounds. (**G**) Quantification of panel **F** (n > 26 from three independent trials). Error bars represent SEM (two-tailed Student's *t*-test, **p* < 0.05). Please note that the RNAi efficiency in our study is similar to that shown by a previous report that generated neuron-specific RNAi strain (Calixto et al. 2010). (**H** and **I**) Photographs of muscle-specific RNAi strain expressing *hlh-1p::pfd-6::RFP* (**H**), and quantification (n > 32, three biological repeats) (**I**).

Figure S4

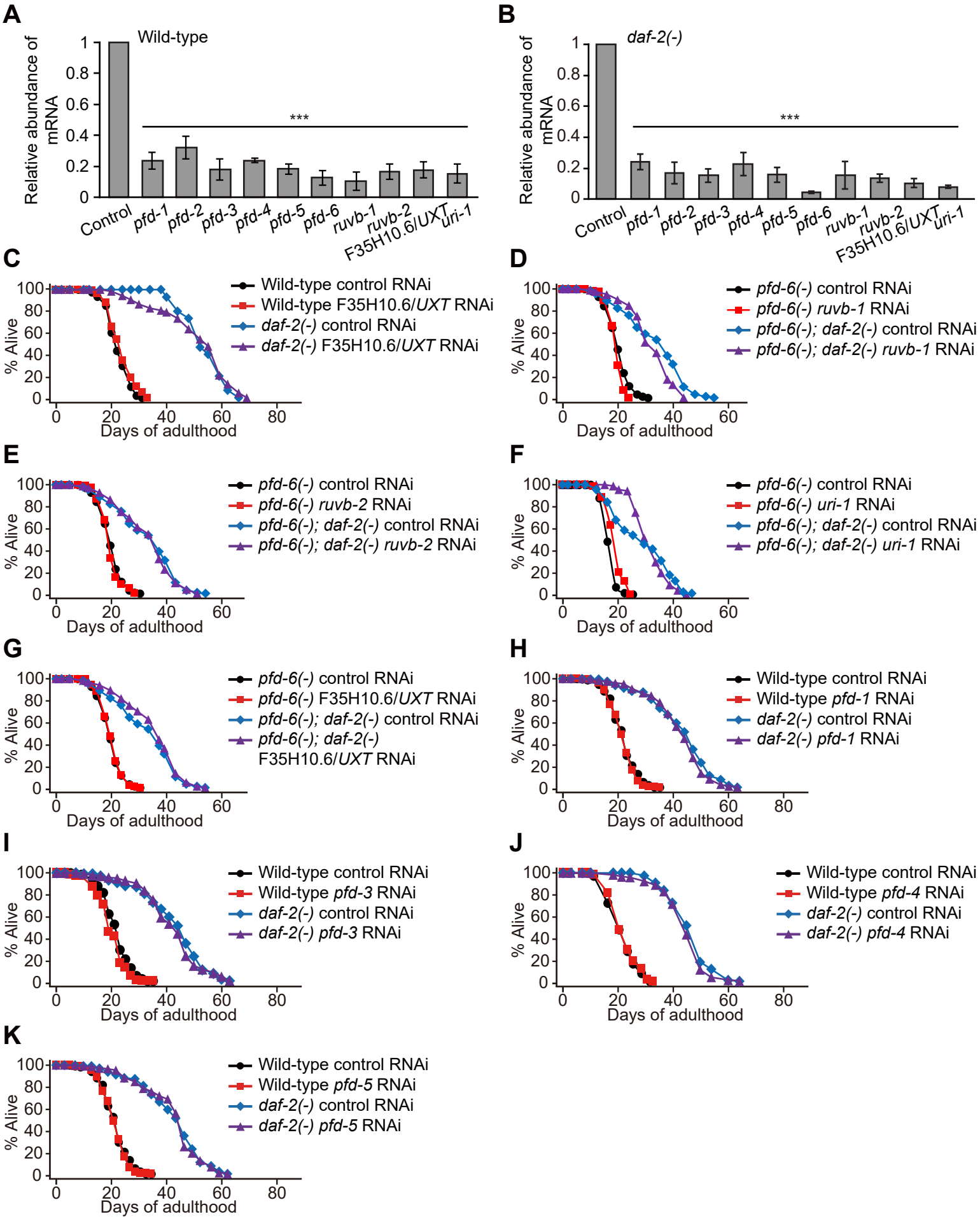
A
Wild-type
Relative abundance of mRNA
1
0.8
0.6
0.4
0.2
0
***
Control
pfd-1
pfd-2
pfd-3
pfd-4
pfd-5
pfd-6
ruvb-1
ruvb-2
F35H10.6/UXT
uri-1
B
daf-2(-)
Relative abundance of mRNA
1
0.8
0.6
0.4
0.2
0
***
Control
pfd-1
pfd-2
pfd-3
pfd-4
pfd-5
pfd-6
ruvb-1
ruvb-2
F35H10.6/UXT
uri-1
C
% Alive
100
80
60
40
20
0
0
20
40
60
80
Days of adulthood
Wild-type control RNAi
Wild-type F35H10.6/UXT RNAi
daf-2(-) control RNAi
daf-2(-) F35H10.6/UXT RNAi
D
% Alive
100
80
60
40
20
0
0
20
40
60
Days of adulthood
pfd-6(-) control RNAi
pfd-6(-) ruvb-1 RNAi
pfd-6(-); daf-2(-) control RNAi
pfd-6(-); daf-2(-) ruvb-1 RNAi
E
% Alive
100
80
60
40
20
0
0
20
40
60
Days of adulthood
pfd-6(-) control RNAi
pfd-6(-) ruvb-2 RNAi
pfd-6(-); daf-2(-) control RNAi
pfd-6(-); daf-2(-) ruvb-2 RNAi
F
% Alive
100
80
60
40
20
0
0
20
40
60
Days of adulthood
pfd-6(-) control RNAi
pfd-6(-) uri-1 RNAi
pfd-6(-); daf-2(-) control RNAi
pfd-6(-); daf-2(-) uri-1 RNAi
G
% Alive
100
80
60
40
20
0
0
20
40
60
Days of adulthood
pfd-6(-) control RNAi
pfd-6(-) F35H10.6/UXT RNAi
pfd-6(-); daf-2(-) control RNAi
pfd-6(-); daf-2(-)
F35H10.6/UXT RNAi
H
% Alive
100
80
60
40
20
0
0
20
40
60
80
Days of adulthood
Wild-type control RNAi
Wild-type pfd-1 RNAi
daf-2(-) control RNAi
daf-2(-) pfd-1 RNAi
I
% Alive
100
80
60
40
20
0
0
20
40
60
80
Days of adulthood
Wild-type control RNAi
Wild-type pfd-3 RNAi
daf-2(-) control RNAi
daf-2(-) pfd-3 RNAi
J
% Alive
100
80
60
40
20
0
0
20
40
60
80
Days of adulthood
Wild-type control RNAi
Wild-type pfd-4 RNAi
daf-2(-) control RNAi
daf-2(-) pfd-4 RNAi
K
% Alive
100
80
60
40
20
0
0
20
40
60
80
Days of adulthood
Wild-type control RNAi
Wild-type pfd-5 RNAi
daf-2(-) control RNAi
daf-2(-) pfd-5 RNAi

Figure S4. The effects of RNAi targeting components of R2TP/prefoldin-like complex and prefoldin complex on lifespan. (**A** and **B**) qRT-PCR results after knocking down each of the components in prefoldin and R2TP/prefoldin-like complexes in wild-type (**A**) and *daf-2(e1370)* (*daf-2(-)*) (**B**) animals. Data were obtained from three biological repeats. Error bars represent SEM (two-tailed Student's *t*-test, ***$p < 0.001$) (**C**) *F35H10.6/UXT* RNAi did not influence the lifespan of wild-type or *daf-2(e1370)* (*(daf-2(-)*) mutants. (**D**-**G**) Inhibition of *ruvb-1* (**D**), *ruvb-2* (**E**), *uri-1* (**F**, one out of two trials), or *F35H10.6/UXT* (**G**) using RNAi did not affect the lifespan of *pfd-6(gk493446); daf-2(e1370)* (*pfd-6(-); daf-2(-)*) animals. (**H**-**K**) RNAi targeting *pfd-1* (**H**), *pfd-3* (**I**), *pfd-4* (**J**) or *pfd-5* (**K**) had no effect on the lifespan of wild-type or *daf-2* mutant animals. See **Supplemental Table S5** for statistical analysis and additional repeats.

Figure S5

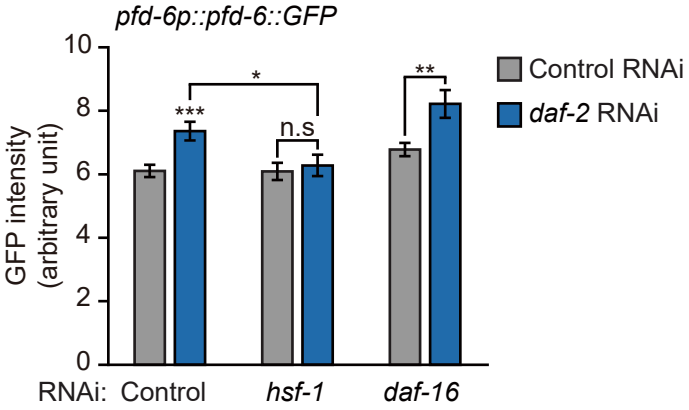
pfd-6p::pfd-6::GFP
GFP intensity (arbitrary unit)
10
8
6
4
2
0
***
*
n.s
**
Control RNAi
daf-2 RNAi
RNAi: Control
hsf-1
daf-16

Figure S5. *daf-2* RNAi increases PFD-6 protein levels in an *hsf-1*-dependent manner. Quantification of PFD-6::GFP levels in control RNAi- and *daf-2* RNAi-treated animals under control RNAi, *hsf-1* RNAi, or *daf-16* RNAi conditions (n > 25, three biological repeats). Error bars represent SEM, and *p* values were calculated by using two-tailed Student's *t*-test (n.s: not significant, *$p < 0.05$, **$p < 0.01$, ***$p < 0.001$). Integrated *pfd-6::GFP* transgenic animals (IJ1249 *yhIs74[pfd-6p::pfd-6::GFP; odr-1p::RFP]*) were used. Here, we performed double RNAi experiments, as integrated *pfd-6::GFP* caused sterility in a *daf-2(e1370)* mutant background.

Figure S6

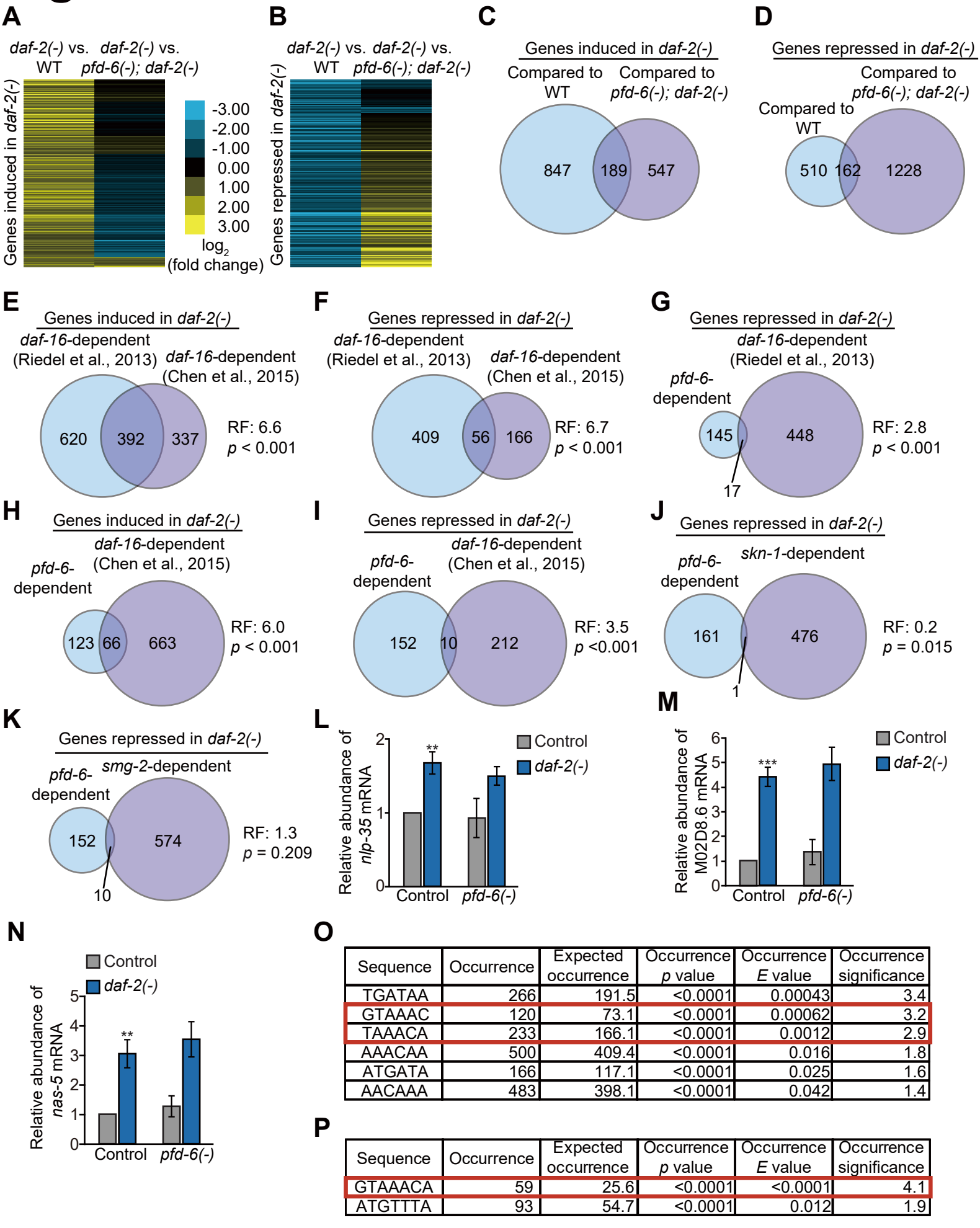

O

Sequence	Occurrence	Expected occurrence	Occurrence *p* value	Occurrence *E* value	Occurrence significance
TGATAA	266	191.5	<0.0001	0.00043	3.4
GTAAAC	120	73.1	<0.0001	0.00062	3.2
TAAACA	233	166.1	<0.0001	0.0012	2.9
AAACAA	500	409.4	<0.0001	0.016	1.8
ATGATA	166	117.1	<0.0001	0.025	1.6
AACAAA	483	398.1	<0.0001	0.042	1.4

P

Sequence	Occurrence	Expected occurrence	Occurrence *p* value	Occurrence *E* value	Occurrence significance
GTAAACA	59	25.6	<0.0001	<0.0001	4.1
ATGTTTA	93	54.7	<0.0001	0.012	1.9

Figure S6. The effects of genetic inhibition of *pfd-6* on the transcriptome of *daf-2* mutants. (**A** and **B**) Heat maps show different expression patterns between up- (**A**, fold change > 1.50 and *p* value < 0.05) and down- (**B**, fold change < 0.67 and *p* value < 0.05, left) regulated genes in *daf-2(e1370)* (*daf-2(-)*) mutants and wild-type animals compared with those in *pfd-6(-); daf-2(-)* double mutants. (**C** and **D**) Venn diagrams show that the expression of 189 genes was up-regulated (**C**) and that of 162 genes was down-regulated (**D**) by *daf-2(-)* mutations in a *pfd-6*-dependent manner (RF: representation factor). *p* values for overlap of Venn diagrams were calculated with hypergeometric probability test. (**E** and **F**) Venn diagrams showing induced (**E**) or repressed (**F**) genes by *daf-2(-)* mutations in a *daf-16*-dependent manner using two previously published RNA-seq. data (Riedel et al. 2013; Chen et al. 2015). (**G**) Venn diagrams show an overlap between genes repressed in *daf-2(-)* mutants that are dependent on PFD-6 and those that are dependent on DAF-16 (Riedel et al. 2013)**.** (**H** and **I**) Venn diagrams indicate overlapping genes between PFD-6-dependent and DAF-16-dependent genes (Chen et al. 2015), whose levels are induced (**H**) or repressed (**I**) in *daf-2(-)* mutants. (**J** and **K**) Shown are the overlaps between PFD-6 targets and SKN-1 targets (Ewald et al. 2015) (**J**), or PFD-6 targets and SMG-2 targets (Son et al. 2017) (**K**), whose expression was repressed in *daf-2(-)* mutants. (**L**-**N**) mRNA levels of *nlp-35* (**L**), M02D8.6 (**M**) and *nas-5* (**N**) were measured by using qRT-PCR (n > 3, error bars represent SEM and *p* values were calculated by using two-tailed Student's *t*-test, ***p* < 0.01, ****p* < 0.001). (**O** and **P**) Shown are motifs containing oligolength of 6 (**O**) and 7 (**P**) that are significantly overrepresented in 800 bp upstream of the coding regions of *pfd-6*-dependent up-regulated genes in *daf-2(-)* mutants. We performed a DNA pattern search with known motifs of transcription factors in insulin/IGF-1 signaling pathway; DAF-16-associated sites (also known as PQM-1/GATA-like binding sites; GAKAAG: 41.3 %), DAF-16-binding element sites

(GTAAARA: 56.6 %), SKN-1-binding sites (WWTRTCAT: 41.8 %), and HSF-1-binding sites (GGGTGTC and TTCTAGAA: 2.1% and 6.3%, respectively).

Figure S7

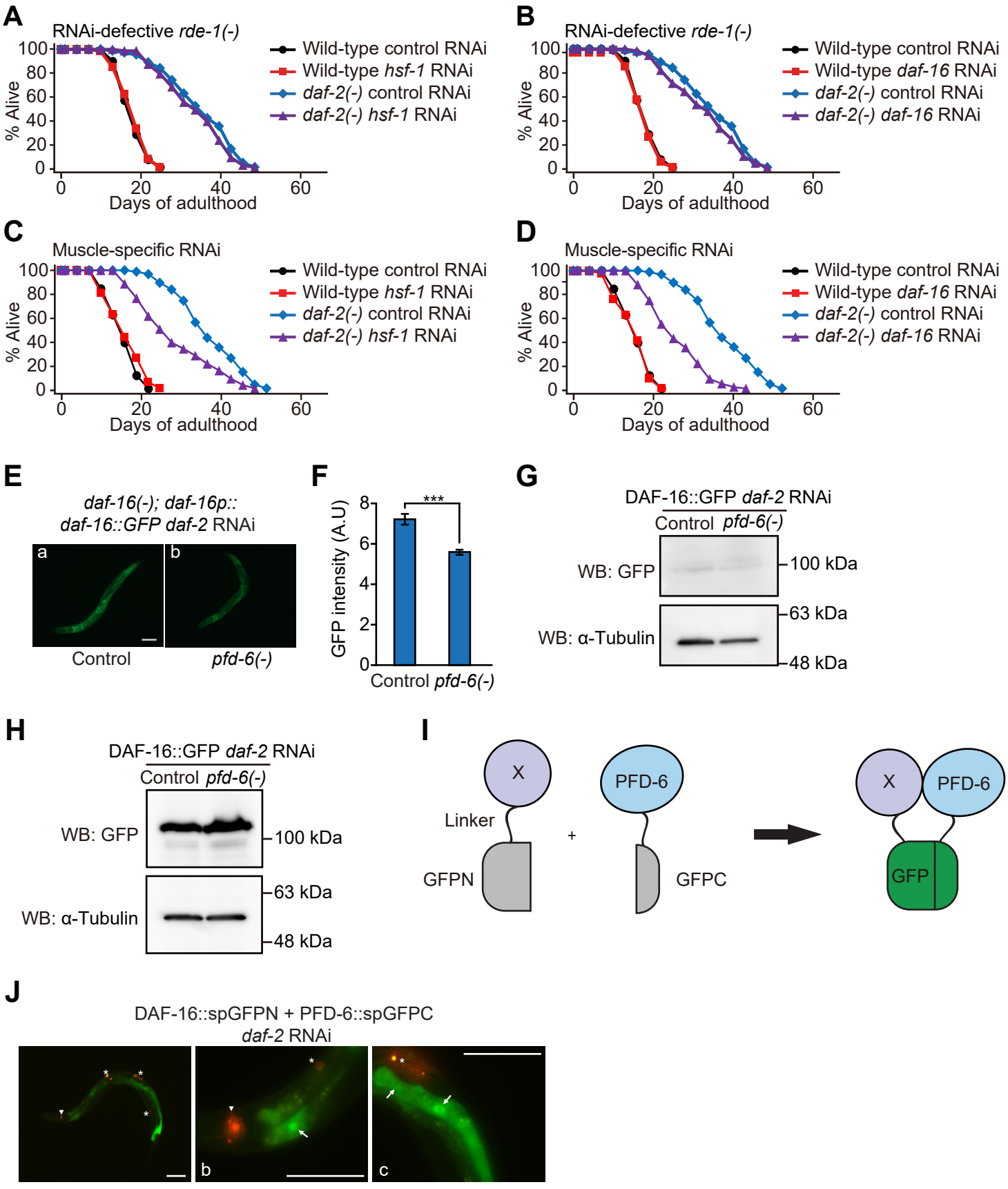
A
RNAi-defective rde-1(-)
% Alive
Days of adulthood
Wild-type control RNAi
Wild-type hsf-1 RNAi
daf-2(-) control RNAi
daf-2(-) hsf-1 RNAi
B
RNAi-defective rde-1(-)
Wild-type control RNAi
Wild-type daf-16 RNAi
daf-2(-) control RNAi
daf-2(-) daf-16 RNAi
C
Muscle-specific RNAi
D
Muscle-specific RNAi
E
daf-16(-); daf-16p::
daf-16::GFP daf-2 RNAi
Control
pfd-6(-)
F
GFP intensity (A.U)
***
G
DAF-16::GFP daf-2 RNAi
WB: GFP
WB: α-Tubulin
100 kDa
63 kDa
48 kDa
H
DAF-16::GFP daf-2 RNAi
I
X
PFD-6
Linker
GFPN
GFPC
GFP
J
DAF-16::spGFPN + PFD-6::spGFPC
daf-2 RNAi

Figure S7. Tissue-specific *hsf-1* and *daf-16* RNAi lifespan assays. (**A** and **B**) *hsf-1* RNAi (**A**) and *daf-16* RNAi (**B**) did not affect the lifespan of RNAi-defective *rde-1(ne219)* (*rde-1(-)*) and *rde-1(ne219); daf-2(e1370)* (*rde-1(-); daf-2(-)*) mutants. (**C** and **D**) Muscle specific *hsf-1* RNAi (**C**) or *daf-16* (**D**) RNAi decreased the longevity of *daf-2(-)* mutants. See **Supplemental Table S6** for statistical analysis and additional repeats. (**E**) DAF-16::GFP levels were decreased by *pfd-6(gk493446)* (*pfd-6(-)*) mutations under *daf-2* RNAi-treated conditions. IJ1058 (*daf-16(mu86); muIs112[daf-16p::GFP::daf-16cDNA; odr-1p::RFP]*) (control) and IJ1230 *pfd-6(gk493446) daf-16(mu86); muIs112[daf-16p::GFP::daf-16cDNA; odr-1p::RFP]* (*pfd-6(-)*) were used. (**F**) Quantification of DAF-16::GFP levels in panel **E** (n > 22 from three independent experiments). Error bars indicate SEM (two-tailed Student's *t*-test, *** $p < 0.001$). Scale bars indicate 100 μm. (**G**) Western blot assays using IJ1058 and IJ1230 strains. DAF-16::GFP was barely detected. WB: Western blot. (**H**) Western blot assays using TJ356 strain (*zIs356[daf-16p::daf-16a/b::GFP; rol-6]*) and IJ1125 *pfd-6(gk493446); zIs356[daf-16p::daf-16::GFP; rol-6D]* indicated that mutations in *pfd-6* did not decrease DAF-16::GFP levels under *daf-2* RNAi conditions (three biological replicates). We speculate that the difference between the results shown in panels **E** and **H** may have originated from using two different *daf-16::GFP* transgenic strains. Therefore, it will be important to measure endogenous DAF-16 levels in future studies. (**I**) A schematic drawing showing a split GFP system for protein-protein interaction. PFD-6 fused with the C-terminal part of GFP and protein X fused with the N-terminal part of GFP are co-expressed. If PFD-6 and protein X interact with each other, green fluorescence is detected. (**J**) Fluorescence images of the N-terminal domain of split GFP fused with DAF-16 isoform a (DAF-16::spGFPN) and PFD-6 fused with the C-terminal domain of split GFP (PFD-6::spGFPC) in *daf-2* RNAi-treated conditions. Triangles indicate *odr-1p::RFP*, a co-injection marker for DAF-

16::spGFPN. Asterisks indicate *unc-122p::RFP*, a co-injection marker for PFD-6::spGFPC. Arrows indicate DAF-16::GFPN and PFD-6:GFPC that bound in the nucleus.

Figure S8

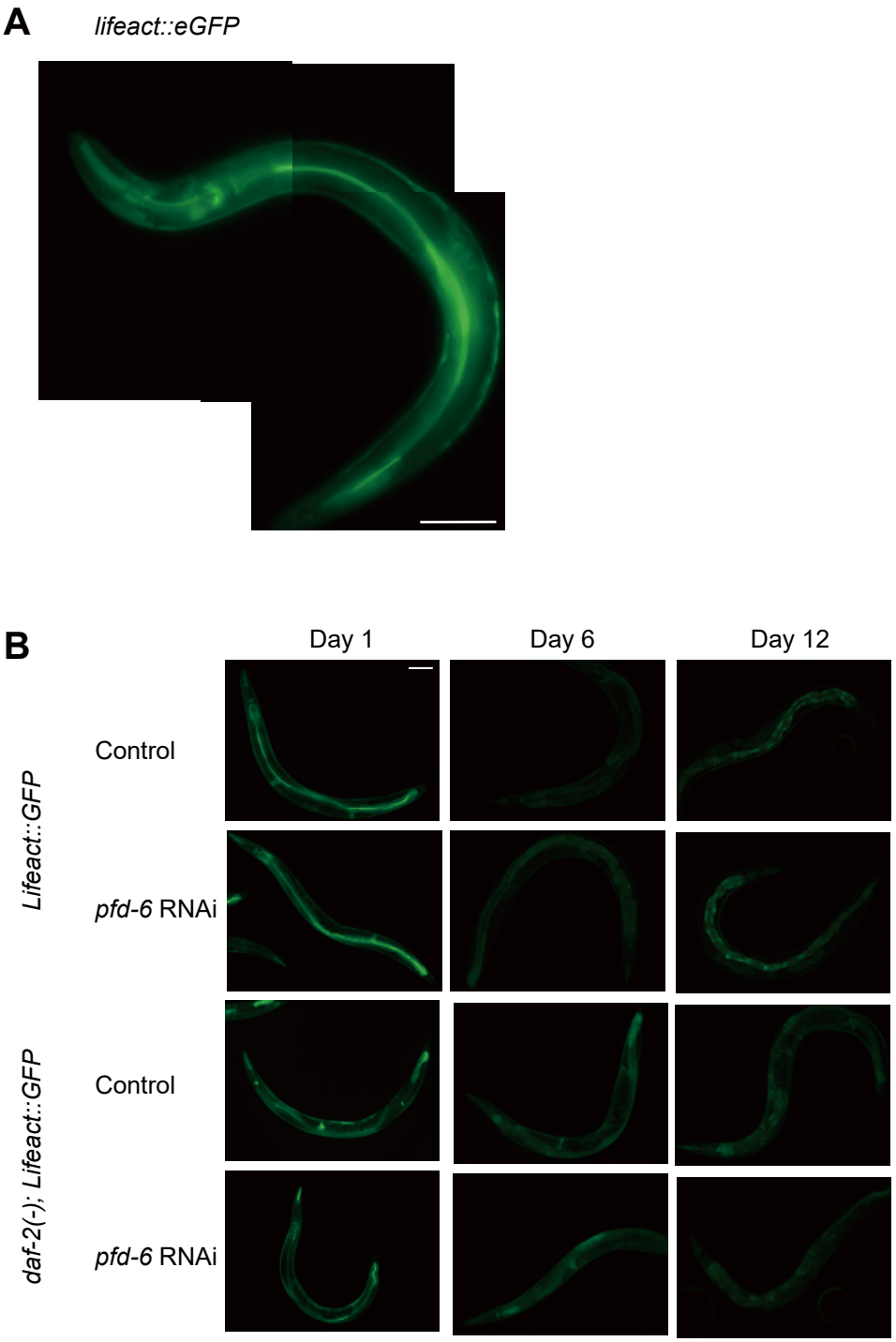
A
lifeact::eGFP
B
Day 1
Day 6
Day 12
Control
pfd-6 RNAi
Lifeact::GFP
Control
pfd-6 RNAi
daf-2(-); Lifeact::GFP
C
% Worms with GFP in the intestinal lumen
100
80
60
40
20
0
Day 1
Day 6
Day 12
Day 18
Wild-type control RNAi
daf-2(-) control RNAi
Wild-type pfd-6 RNAi
daf-2(-) pfd-6 RNAi

Figure S8. *pfd-6* RNAi did not affect the enhanced maintenance of actin proteins in *daf-2* mutants during aging.

(**A**) Lifeact::GFP, which binds actin filaments, was detected in the intestinal lumen. (**B**) Fluorescence images of *Lifeact::GFP*-expressing worms in wild-type or *daf-2(e1370)* (*daf-2(-)*) backgrounds treated with *pfd-6* RNAi during aging. (**C**) Quantification of panel **B**. Error bars represent SEM (n > 18 from three independent experiments).

Figure S9

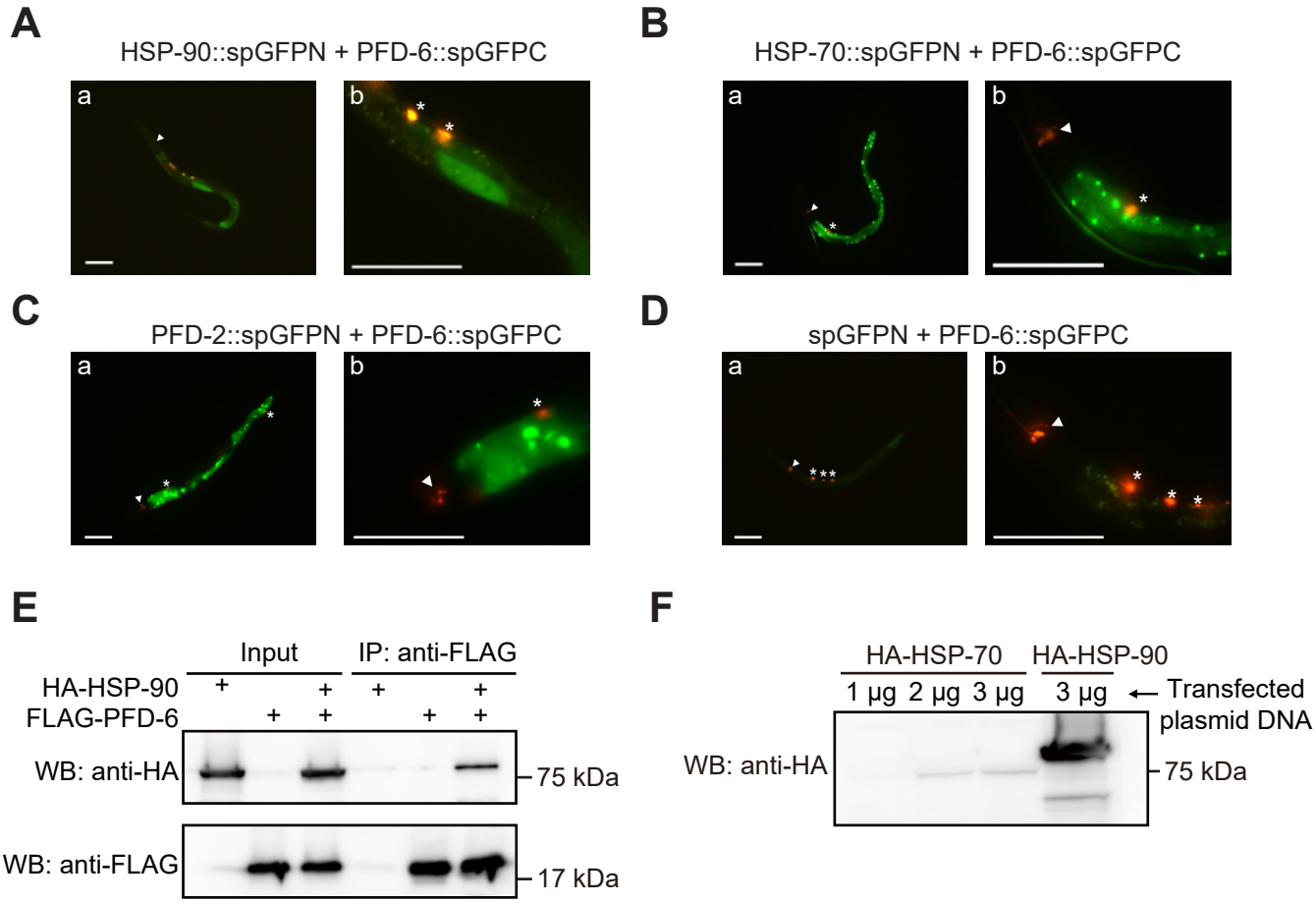
A
HSP-90::spGFPN + PFD-6::spGFPC
a
b
B
HSP-70::spGFPN + PFD-6::spGFPC
a
b
C
PFD-2::spGFPN + PFD-6::spGFPC
a
b
D
spGFPN + PFD-6::spGFPC
a
b
E
Input
IP: anti-FLAG
HA-HSP-90
FLAG-PFD-6
WB: anti-HA
75 kDa
WB: anti-FLAG
17 kDa
F
HA-HSP-70
HA-HSP-90
1 µg 2 µg 3 µg
3 µg
Transfected plasmid DNA
WB: anti-HA
75 kDa

Figure S9. PFD-6 binds HSP-90 and HSP-70.

(**A-D**) Pictures of worms expressing C-terminal GFP fused with PFD-6 (PFD-6::GFPC) and N-terminal GFP fused with HSP-90::spGFPN (**A**), HSP-70 (HSP-70::spGFPN) (**B**), PFD-2::spGFPN (**C**) and spGFPN (**D**) (scale bars: 100 μm). *vha-6* promoter, an intestine-specific promoter, was used for expressing split GFP-fused proteins. Triangles indicate *odr-1p::RFP*, a co-injection marker for HSP-70::spGFPN, HSP-90::spGFPN, spGFPN or PFD-2::spGFPN. Asterisks indicate *unc-122p::RFP*, a co-injection marker for PFD-6::spGFPC. (**E**) Co-immunoprecipitation (Co-IP) assays with HA-HSP-90 and FLAG-PFD-6 using HEK 293T cells (three independent repeats). WB indicates Western blot. (**F**) Western blot assays were performed to determine the expression of HA-HSP-70 in cultured mammalian cells. The level of HSP-70 was very low, and therefore we were not able to perform co-immunoprecipitation assay with HSP-70. We speculate that codon usage or other unknown factors may have affected the expression of *C. elegans* HSP-70 in cultured mammalian cells. HA-HSP-90 was used as a positive control.

Supplemental references

Calixto A, Chelur D, Topalidou I, Chen X, Chalfie M. 2010. Enhanced neuronal RNAi in *C. elegans* using SID-1. *Nature methods* **7**: 554-559.

Chen AT, Guo C, Itani OA, Budaitis BG, Williams TW, Hopkins CE, McEachin RC, Pande M, Grant AR, Yoshina S et al. 2015. Longevity Genes Revealed by Integrative Analysis of Isoform-Specific daf-16/FoxO Mutants of Caenorhabditis elegans. *Genetics* **201**: 613-629.

Ewald CY, Landis JN, Porter Abate J, Murphy CT, Blackwell TK. 2015. Dauer-independent insulin/IGF-1-signalling implicates collagen remodelling in longevity. *Nature* **519**: 97-101.

Riedel CG, Dowen RH, Lourenco GF, Kirienko NV, Heimbucher T, West JA, Bowman SK, Kingston RE, Dillin A, Asara JM et al. 2013. DAF-16 employs the chromatin remodeller SWI/SNF to promote stress resistance and longevity. *Nature cell biology* **15**: 491-501.

Son HG, Seo M, Ham S, Hwang W, Lee D, An SW, Artan M, Seo K, Kaletsky R, Arey RN et al. 2017. RNA surveillance via nonsense-mediated mRNA decay is crucial for longevity in daf-2/insulin/IGF-1 mutant *C. elegans*. *Nature communications* **8**: 14749.